AMERICAN SOCIETY FOR MICROBIOLOGY | Applied and Environmental Microbiology®

ENVIRONMENTAL MICROBIOLOGY

Unusual Versatility of the Filamentous, Diazotrophic Cyanobacterium *Anabaena torulosa* Revealed for Its Survival during Prolonged Uranium Exposure

Celin Acharya,[a,c] Pallavi Chandwadkar,[a] Chandrani Nayak[b]

Molecular Biology Division, Bhabha Atomic Research Centre, Trombay, Mumbai, India[a]; Atomic and Molecular Physics Division, Bhabha Atomic Research Centre, Trombay, Mumbai, India[b]; Homi Bhabha National Institute, Anushakti Nagar, Mumbai, India[c]

ABSTRACT Reports on interactions between cyanobacteria and uranyl carbonate are rare. Here, we present an interesting succession of the metabolic responses employed by a marine, filamentous, diazotrophic cyanobacterium, *Anabaena torulosa* for its survival following prolonged exposure to uranyl carbonate extending up to 384 h at pH 7.8 under phosphate-limited conditions. The cells sequestered uranium (U) within polyphosphates on initial exposure to 100 μM uranyl carbonate for 24 to 28 h. Further incubation until 120 h resulted in (i) significant degradation of cellular polyphosphates causing extensive chlorosis and cell lysis, (ii) akinete differentiation followed by (iii) extracellular uranyl precipitation. X-ray diffraction (XRD) analysis, fluorescence spectroscopy, X-ray absorption near edge structure (XANES), and extended X-ray absorption fine structure (EXAFS) spectroscopy established the identity of the bioprecipitated uranium as a U(VI) autunite-type mineral, which settled at the bottom of the vessel. Surprisingly, *A. torulosa* cells resurfaced as small green flakes typical of actively growing colonies on top of the test solutions within 192 to 240 h of U exposure. A consolidated investigation using kinetics, microscopy, and physiological and biochemical analyses suggested a role of inducible alkaline phosphatase activity of cell aggregates/akinetes in facilitating the germination of akinetes leading to substantial regeneration of *A. torulosa* by 384 h of uranyl incubation. The biomineralized uranium appeared to be stable following cell regeneration. Altogether, our results reveal novel insights into the survival mechanism adopted by *A. torulosa* to resist sustained uranium toxicity under phosphate-limited oxic conditions.

IMPORTANCE Long-term effects of uranyl exposure in cyanobacteria under oxic phosphate-limited conditions have been inadequately explored. We conducted a comprehensive examination of the metabolic responses displayed by a marine cyanobacterium, *Anabaena torulosa*, to cope with prolonged exposure to uranyl carbonate at pH 7.8 under phosphate limitation. Our results highlight distinct adaptive mechanisms harbored by this cyanobacterium that enabled its natural regeneration following extensive cell lysis and uranium biomineralization under sustained uranium exposure. Such complex interactions between environmental microbes such as *Anabaena torulosa* and uranium over a broader time range advance our understanding on the impact of microbial processes on uranium biogeochemistry.

KEYWORDS biomineralization, cyanobacteria, phosphatase, polyphosphates, regeneration, uranium

Received 13 December 2016 **Accepted** 19 February 2017

Accepted manuscript posted online 3 March 2017

Citation Acharya C, Chandwadkar P, Nayak C. 2017. Unusual versatility of the filamentous, diazotrophic cyanobacterium *Anabaena torulosa* revealed for its survival during prolonged uranium exposure. Appl Environ Microbiol 83:e03356-16. https://doi.org/10.1128/AEM.03356-16.

Editor Robert M. Kelly, North Carolina State University

Address correspondence to Celin Acharya, celin@barc.gov.in.

Microorganisms have existed on earth for at least 3.5 billion years (1) and are the most successful life forms to date (2). They have been exposed to their immediate environments comprising essential elements or complex mixtures of naturally occur-

ring toxic elements. Microbes have evolved metabolic responses to circumvent metal toxicity, which have facilitated their growth and survival in metal-contaminated environments (3, 4).

Research on the influence of actinide elements such as uranium on microorganisms is still in its infancy. Uranyl interactions with different microbial processes have led to the formation of a broad range of biogenic materials, such as uranyl oxides, phosphates, and carbonates, which are currently being explored in the context of nuclear waste isolation (5). The microbial cells protect themselves against uranium toxicity through different mechanisms, including bioadsorption (through ligands), intracellular accumulation, bioprecipitation, and bioreduction, which have been documented extensively (6–9). The reduction of uranium(VI) [U(VI)] to U(IV) by Fe(III) and sulfate-reducing bacteria was proposed to prevent the migration of uranium in contaminated waters (10–13), wherein U(VI) reduction resulted in extracellular precipitation of U(IV) mineral uraninite or monomeric U(IV) (10, 14). The contribution of phosphate ligands generated either by the action of phosphatase enzymes on organophosphate substrates or by polyphosphate (polyP) degradation has been demonstrated with respect to redox-independent bacterial uranium precipitation as uranyl phosphate minerals (15–18). A *Citrobacter* sp. (since reassigned *Serratia* species) was shown to precipitate uranium under physiological conditions (pH 6.9) as cell-bound uranyl phosphate via enzymatically generated phosphate ligands (15, 16). A recombinant *Deinococcus radiodurans* strain overexpressing alkaline phosphatase (PhoK) precipitated uranium from dilute alkaline solutions at pH 9 (17). In bacterial cells, polyphosphate, a phosphate polymer, has been implicated in sequestering toxic metals intracellularly and improving cellular resistance to metals (19). The intracellular accumulation of U in polyphosphates was observed in various bacterial strains isolated from uranium mining wastes, including *Acidithiobacillus ferrooxidans*, *Sphingomonas* sp., and *Pseudomonas migulae* (6, 20, 21). There is no evidence for uranium transporters, and its passage into microbial cells occurs through passive diffusion due to an increased membrane permeability resulting from uranium toxicity (22). Such intracellular sequestration within phosphate-rich granules or polyphosphates decreases the intracellular U concentration thereby protecting sensitive cytosolic molecules from U toxicity (6, 20, 21). On the other hand, the hydrolysis or degradation of polyphosphates in response to heavy metals or nutrient stress has been proposed to precipitate heavy metals extracellularly, enabling metal detoxification (23, 24). The overexpression of the polyphosphate kinase (*ppk*) gene in *Pseudomonas aeruginosa* results in the significant accumulation of polyphosphates which degrade under carbon-starved conditions, and the phosphates released therefrom precipitate uranyl out of the solutions (24). Several environmental strains, such as *Cellulomonas*, *Arthrobacter*, *Rahnella*, and *Bacillus*, isolated from contaminated subsurface soils of the Department of Energy's Field Research Centre (ORFRC) were shown to immobilize uranium as a biogenic phosphate mineral resulting from polyphosphate metabolism or organophosphate hydrolase activity (25–27).

Previous studies on uranium bioremediation/biomineralization have focused on the bacterial reduction of U(VI) to uraninite or monomeric U(IV) under anoxic conditions or on enzymatic bioprecipitation in the presence of exogenous organic phosphate substrate under oxic conditions (15, 25, 27–29) and anoxic conditions (30) below a circumneutral pH. However, much of the uranyl contamination found in groundwater/aquatic systems exists above a circumneutral pH where uranyl mobility is predominantly controlled by carbonates through the formation of highly soluble and stable uranyl carbonate complexes (31). Such aquatic and contaminated environments are suggested to be low in phosphate availability (32–34). The microbes inhabiting environments with low phosphate availability employ a high-affinity phosphate transport system for phosphate introduction into the cells (34–36). Cyanobacteria, a dominant component of aquatic environments, have been shown to synthesize alkaline phosphatases (APases) during prolonged periods of phosphorus deprivation, which catalyze the degradation of various complex organic phosphate substrates into biologically available inorganic phosphate (Pi) at an alkaline pH (37). Furthermore, these organisms

are exposed to direct and indirect contaminants and have evolved various molecular and physiological adaptations to cope with contaminant toxicity in aquatic systems (8).

Information is limited on redox-independent cyanobacterial responses to soluble uranyl carbonate complexes under phosphate-limited conditions and over a broad time range. The present investigation elucidates the distinct metabolic responses demonstrated by a filamentous, heterocystous, nitrogen-fixing marine cyanobacterium, *Anabaena torulosa* (belonging to *Nostocales*), for alleviating immediate and sustained *in situ* U toxicity, simultaneously safeguarding its growth and survival under phosphate-limited U exposure conditions extending up to 384 h. *Anabaena torulosa* is a heterocyst-forming photoautotrophic cyanobacterium that grows in long filaments of vegetative cells. Two types of specialized cells may be present in various numbers within a filament of vegetative cells, (i) the nitrogen fixing cells or heterocysts and (ii) resting cells or akinetes (formed under stressed conditions), which are larger than vegetative cells (38). This organism is reported to be highly tolerant to osmotic stress and ionizing radiation (39, 40). The present study lends important insights into the physiological and biochemical adaptations displayed by *A. torulosa* to resist prolonged uranium contamination.

RESULTS

Cell lysis, akinete differentiation, and chlorosis in uranium-exposed *A. torulosa* culture. Cells exposed to uranium for 24 h revealed distinct, dense dark granules (Fig. 1A, indicated by arrows) in comparison to the control U-unchallenged cells. Exposure of *A. torulosa* to 100 μM U for $\geq$36 h caused cell lysis followed by akinete differentiation by 96 h (Fig. 1A, indicated by arrows) of uranyl incubation under phosphate-limited conditions. Incubations for $\geq$96 h in the presence of 100 μM U resulted in cell aggregates comprising isolated heterocysts, lysed vegetative filaments, and spores/akinetes (detached from their trichomes) (Fig. 1A). By contrast, akinete differentiation without any appreciable cell lysis was visualized in the control U-unchallenged culture only by 384 h of incubation under identical conditions of phosphate limitation (Fig. 1B), suggesting that uranium toxicity coupled with phosphate limitation prompted the cell lysis and akinete formation as early as 96 h in the uranium-exposed culture.

The cells demonstrated significant bleaching within 120 to 144 h of 100 μM U exposure (Fig. 1C and D). The chlorophyll *a* contents of U-exposed cells reduced drastically from 5.2 μg ml^{-1} to an almost negligible level, i.e., 0.02 μg ml^{-1} within 144 h of U exposure (Fig. 1C), whereas the control U-unchallenged cells showed an increase in chlorophyll *a* contents (5.4 to 9.56 μg ml^{-1}) during the same period (Fig. 1C and D). The observed chlorosis in U-exposed *A. torulosa* cells was most likely due to the degradation of photosynthetic pigments and is a known consequence of heavy-metal exposure in cyanobacteria (41). Previously, we witnessed ~10% inhibition in the growth of this strain when exposed to 100 μM U for 24 to 30 h compared with that in control U-unexposed conditions (42). No cell lysis was observed and the chlorophyll *a* contents did not change measurably within 24 to 30 h of U exposure under phosphate-limited conditions (Fig. 1A and C), which is in agreement with previous findings (42). However, exposure to 100 μM U for $\geq$36 h resulted in cell lysis and chlorosis in these cells, as evidenced in this study.

Characteristic features of spores or akinetes in U-exposed *A. torulosa*. The akinetes formed in U-challenged *A. torulosa* culture possessed thick walls and appeared larger in size than the vegetative cells (Fig. 2A). Early stage akinetes in a U-exposed culture (96 h) examined using fluorescence microscopy revealed red chlorophyll *a* fluorescence (λ, 680 nm) upon excitation with green light (λ, 520 nm) (Fig. 2A), similar to that observed in vegetative cells. By contrast, chlorophyll *a* fluorescence of akinetes was observed to be highly quenched in 168 h U-exposed culture (Fig. 2A), consistent with the formation of matured akinetes by different species of the filamentous heterocystous cyanobacteria belonging to *Nostocales* (43). Laser scanning confocal microscopy of DAPI (4′,6-diamidino-2-phenylindole)-stained 96-h-challenged akinete-bearing culture revealed a strong blue fluorescence in the central part of the akinetes as a result

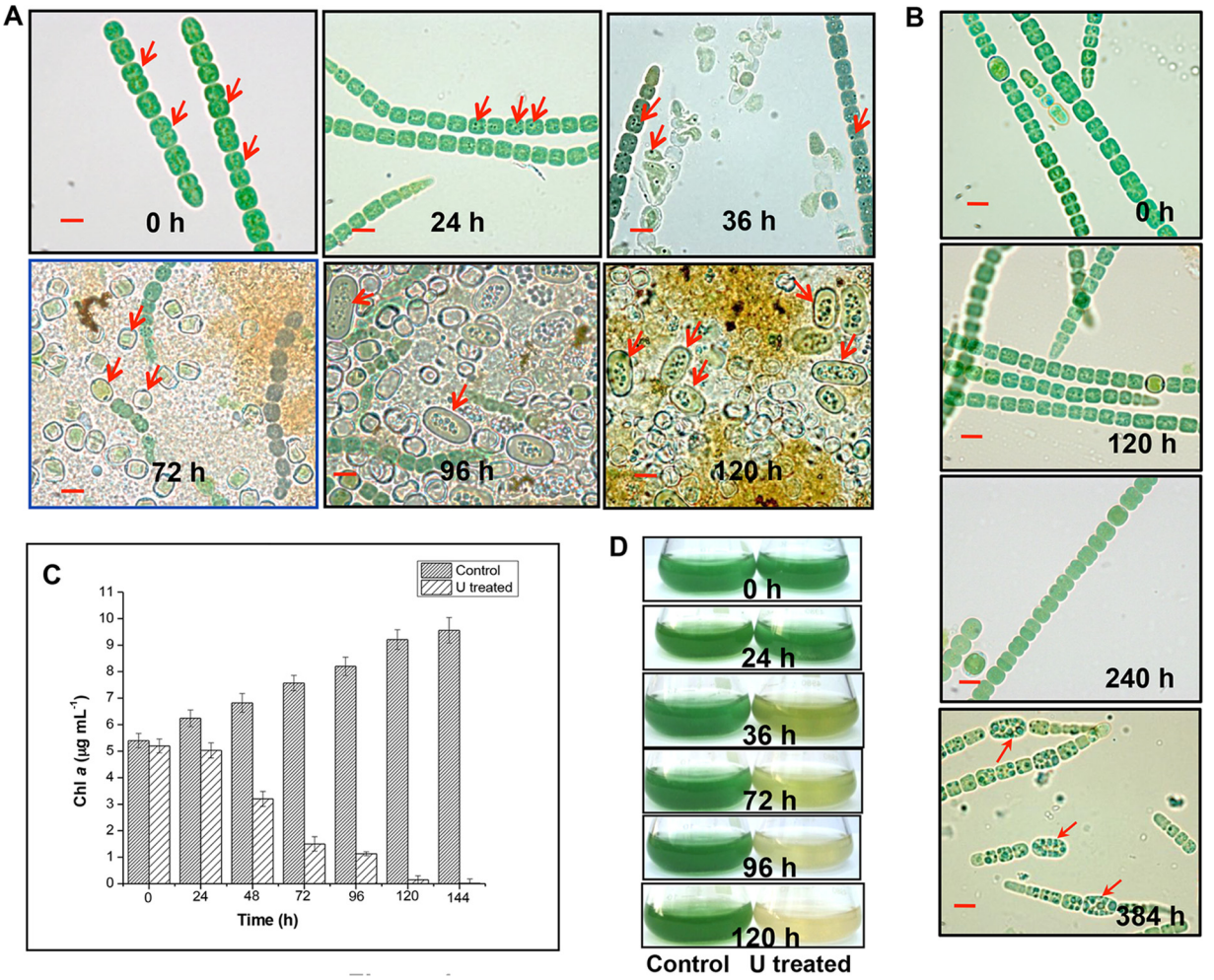

FIG 1 Cell lysis, chlorosis, and akinete differentiation in U-exposed *A. torulosa* culture. Mid-log-phase cells at the equivalent of 0.2 mg (dry weight) ml^{-1} were exposed to 100 μM U (A) or unexposed to U (B) at pH 7.8 and were observed under a microscope under bright-field illumination (magnification, ×1,500; bars indicate 5 μm) at regular intervals. The data are a representative of three biological replicates. The red arrows in (A) show vegetative cells at 0 h, the dense dark granules formed as a result of colocalization of uranium with polyphosphate bodies at 24 h and 36 h in vegetative cells, heterocysts at 72 h, and akinetes at 96 h and 120 h. Red arrows in (B) indicate the differentiating akinetes at 384 h of incubation under control, uranium-unexposed phosphate-limited conditions. (C) Growth of U-unexposed control cells or cells exposed to 100 μM uranyl carbonate is represented by chlorophyll *a* (Chl *a*) contents. (D) The flasks containing control or U-challenged *A. torulosa* cultures corresponding to those mentioned in panel C.

of the emission from DAPI bound to DNA (Fig. 2B, indicated by arrows). Following 120 h of U exposure, the bleached and lysed akinete-bearing *A. torulosa* culture resumed its normal growth when spotted on BG-11 agar plates and incubated under optimal conditions of light and temperature, ensuring the viability of the akinetes (Fig. 2C).

Polyphosphate degradation and uranium bioprecipitation. The hydrolysis of polyphosphate induced in the presence of heavy metals and the free phosphate released at the expense of polyphosphate degradation have been shown to be involved in the extracellular precipitation of heavy metals, including uranium (23, 24, 44, 45). Polyphosphate degradation and phosphate release were observed in an engineered strain of *Pseudomonas aeruginosa* overexpressing the polyphosphate kinase gene (*ppk*) under nutrient starvation conditions, resulting in the removal of 80% soluble U as uranyl phosphate precipitates (24).

The total polyphosphate contents of control and U-challenged *A. torulosa* cells were analyzed to appreciate the role of polyphosphate in mitigating uranium toxicity. Cellular polyphosphate levels in U-challenged cells declined by 50 to 54% within 36 h of U exposure compared with that in control U-unchallenged cells, which did not show

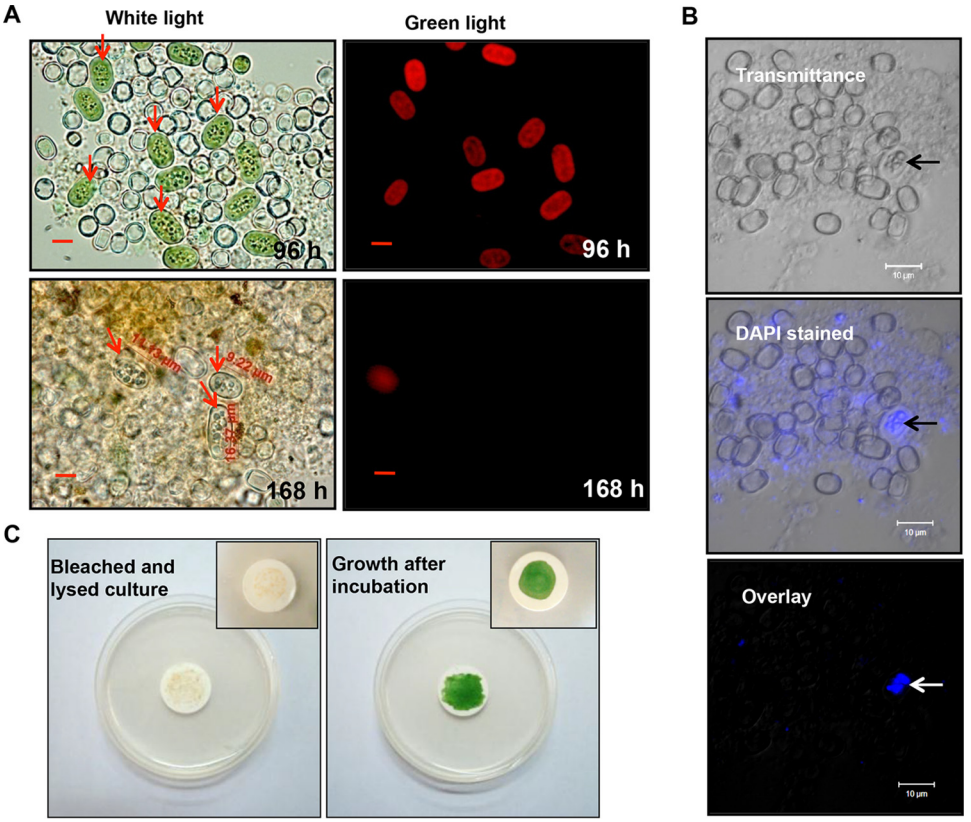

FIG 2 Characteristics of akinetes in U-exposed *A. torulosa* culture. (A) *A. torulosa* cultures showing aggregates of akinetes (red arrows) (and isolated heterocysts) following 96 and 168 h of uranyl (100 μM) exposure were recorded with bright-field microscopy (magnification, $\times$1,500; bars indicate 5 μm) with their respective chlorophyll *a* fluorescence (see the text for details). Akinetes as large as 16.37 μm can be seen in 168-h U-exposed culture. (B) A 96-h, uranyl-exposed akinete-bearing *A. torulosa* culture was stained with DAPI and observed using a laser scanning confocal microscope. The transmitted light image, wavelength color-coded image, and a superposition of both images are presented. Strong blue fluorescence signal (in overlay) indicates the concentration of nucleic acids (indicated with arrows) in the central part of the akinete. The photomicrographs in panels A and B are representative of three biological replicates. (C) The bleached and lysed 120-h U-challenged *A. torulosa* culture was spotted onto filter discs (0.45 μm, MF-Millipore membrane filter; Merck Millipore, Germany), inoculated onto BG-11 agar plates, and incubated under continuous illumination for 168 h. The bleached and lysed culture resumed its normal growth following incubation. The insets show a closer view of the filter discs spotted with *A. torulosa* culture before and after incubation.

any appreciable decrease in their polyphosphate levels during the same period (Fig. 3A). The observations of control cells are in accordance with previous studies where the *ppa* gene encoding the protein involved in the hydrolysis of inorganic phosphate polymers, namely, the inorganic pyrophosphatase PPA, was found to be downregulated in *Anabaena* in response to short-term (5 h) and long-term (6 day) inorganic phosphate (Pi)-starved (no phosphate [P]) conditions, suggestive of non-exploitation of inorganic phosphate storage during this period (46). Microscopic examination of U-challenged cells stained with toluidine blue demonstrated significant degradation of polyphosphate (polyP) within 36 h of U exposure, eventually leading to cell lysis by 120 h (Fig. 3B). No such polyP degradation was visualized in control U-unchallenged cells, even after up to 120 h of incubation (Fig. 3C), suggesting that the presence of uranium under phosphate-limited conditions stimulated the hydrolysis or degradation of polyphosphate in *A. torulosa* as early as 36 h.

Significant amounts of soluble uranium (Fig. 3D) and phosphate (Fig. 3E) were detected in the culture medium by 36 h of uranyl incubation corresponding to ~50% polyphosphate degradation (Fig. 3A) and cell lysis (Fig. 1A and 3B). Limited amounts of soluble phosphate (5 to 7 μM) in the experimental media (BG-11, P negative [P^-]) were observed at the inoculation of the cells (grown in BG-11, P-positive [P^+]) at 0 h in the

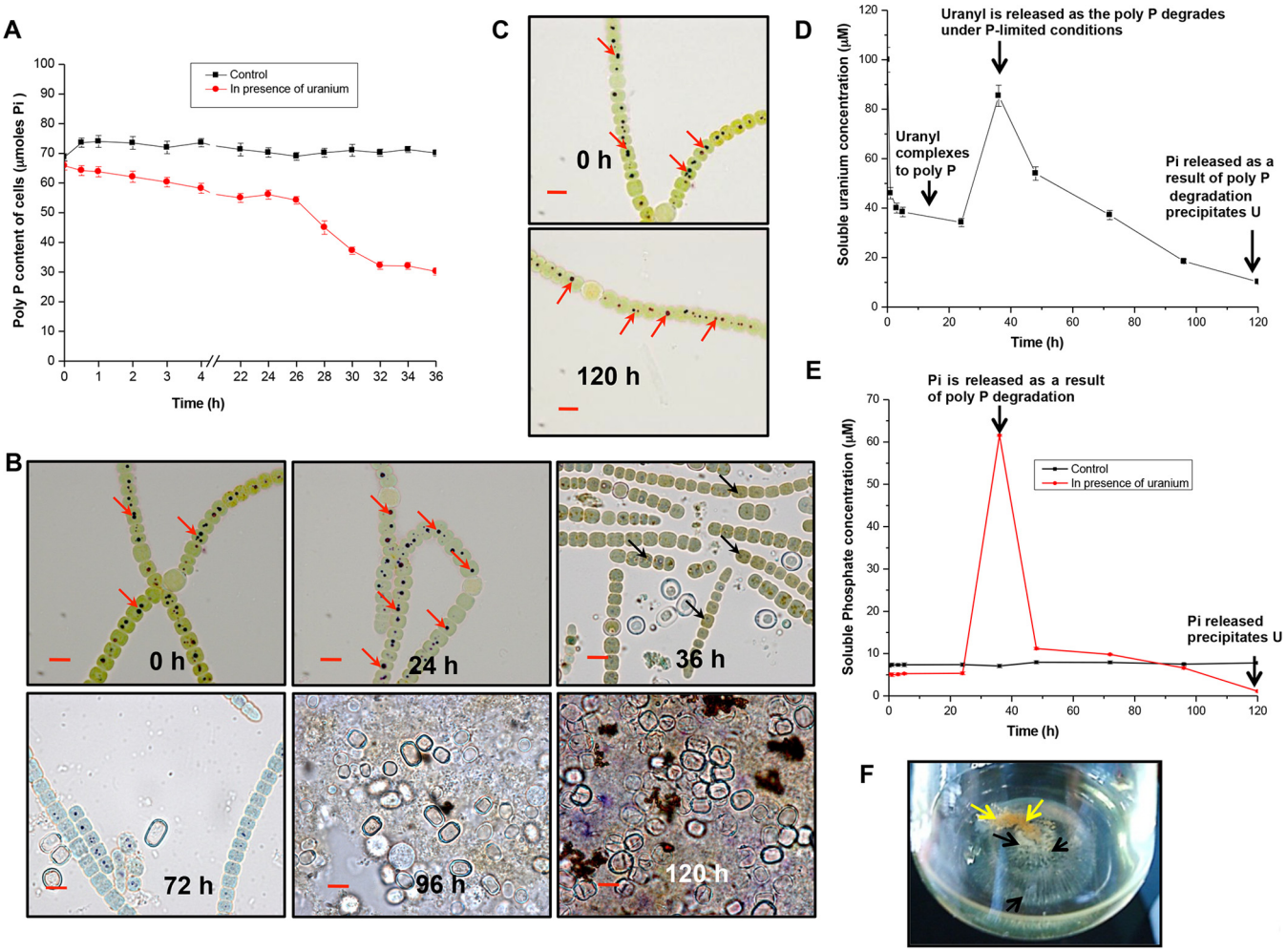

FIG 3 Polyphosphate degradation and uranium bioprecipitation in *A. torulosa*. (A) Mid-log-phase cells at the equivalent of 0.2 mg (dry weight) ml^{-1} were incubated under control conditions or challenged with 100 μM uranyl carbonate wherein the polyP contents of the cells were measured (expressed in μmol Pi per 0.5 optical density at 750 nm [OD_{750}] per liter) until 36 h. (B) Uranyl-challenged cells (extending from 0 h to 120 h) were stained with toluidine blue and were observed with bright-field microscopy using a Carl Zeiss Axioskop 40 microscope with oil-immersion objectives (magnification, ×1,500; bars indicate 5 μm). These correspond to the cells shown in Fig. 1A. Note that the polyphosphates showing a characteristic red color (at 0 h and 24 h, marked by red arrows) degrade by 36 h and appear as dark spots (marked by black arrows). Images corresponding to cells exposed to U for 120 h show lysis following polyP degradation in contrast to control U-unexposed cells (C) stained with toluidine blue showing no such polyphosphate (marked by red arrows) degradation. (D and E) Soluble uranium (in U-exposed culture) (D) and soluble phosphate (E) concentrations in control and U-exposed cultures during 120 h of incubation. (F) Flask displaying the uranium precipitates formed by *A. torulosa* cells following 120 h of U exposure. The layer of yellowish uranyl precipitates that settled at the bottom of the flask is indicated by black arrows underneath the brownish cell aggregates comprising bleached and degraded *A. torulosa* cells (yellow arrows).

absence or presence of uranium (Fig. 3E). The switch of the cyanobacterial cells from P^+ to P^- conditions might have resulted in minor polyphosphate degradation leading to the observed phosphate release. The soluble phosphate increased from 5.16 μM (at 0 h) to ~62 μM within 36 h of U exposure in contrast to that in the control U-unchallenged culture under identical conditions where the phosphate level was almost constant during 120 h of incubation (Fig. 3E). Free phosphate and soluble U concentrations steadily decreased along with the progression of uranyl incubation and were almost negligible by 120 h (Fig. 3D and E). The reactive phosphate precipitated ~88% of the soluble uranium out of the solution within 120 h (Fig. 3D). The precipitated uranium appeared as a layer of yellowish, fine-crystalline powdery material settled at the bottom of the flask underneath the cell aggregates of bleached and decomposed *A. torulosa* culture following 120 h of uranyl exposure (Fig. 3F).

Characterization of bioprecipitated uranium. X-ray powder diffraction (XRD) analysis of the uranium precipitates formed by *A. torulosa* cells after 120 h of U

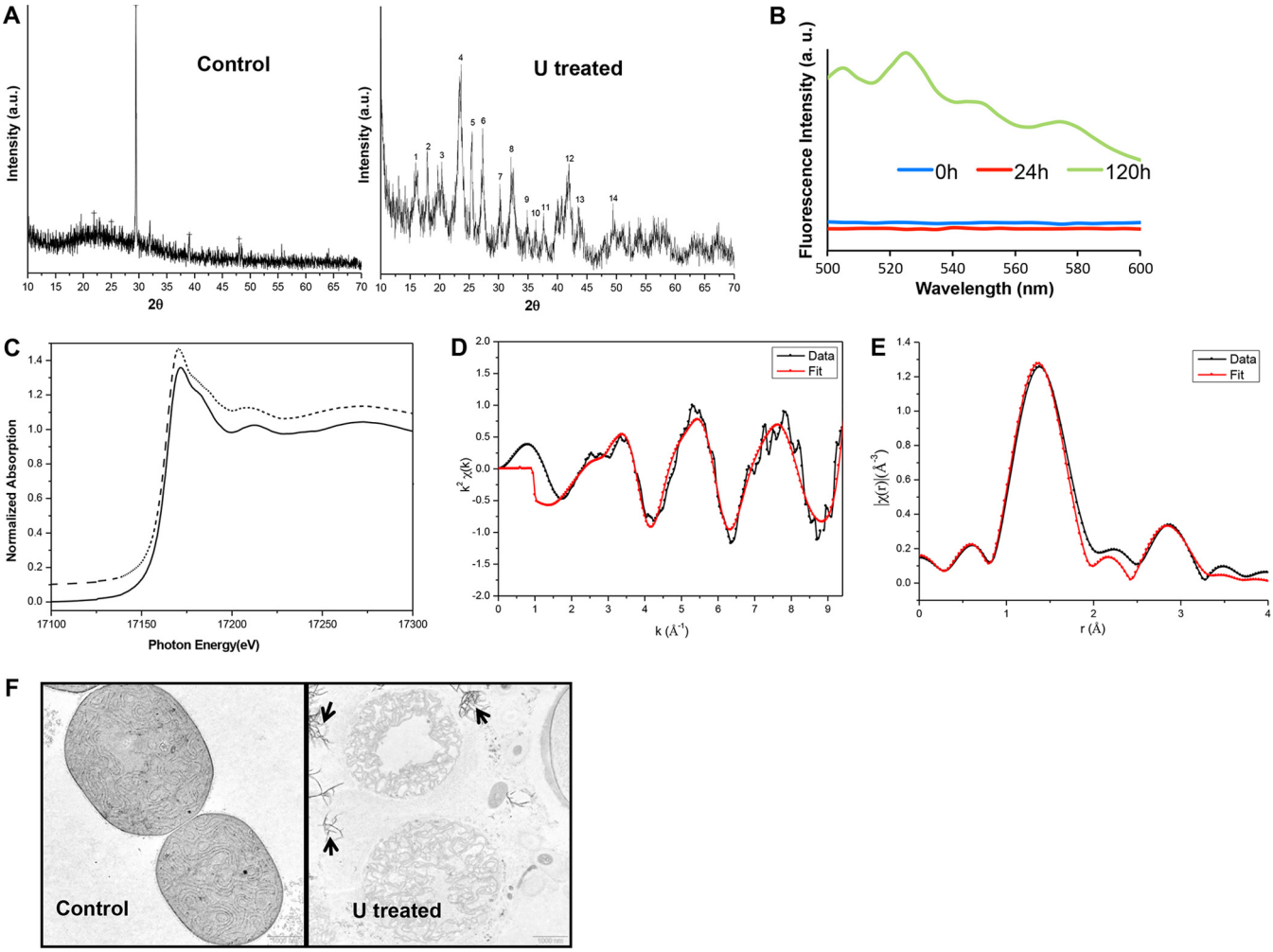

FIG 4 Characterization of bioprecipitated uranium. (A) XRD spectra of *A. torulosa* cells before and after 120 h of exposure to 100 μM uranyl carbonate. (B) Time-resolved fluorescence spectra of *A. torulosa* cells following 0 h, 24 h, and 120 h of uranium confrontation. The peaks at 505, 526, 550, and 575 nm, characteristic of chernikovite/meta-autunite, were observed for 120-h uranyl-exposed cells. (C) Normalized uranium L_{III} edge XANES spectra of 10^{-3} M U(VI) in 1 M $HClO_4$ (dotted line) and 120-h uranyl-exposed cells (solid line). (D and E) Uranium L_{III} edge k^2-weighted EXAFS spectrum (D) and corresponding FT (E) of uranium complexes formed by 120-h U-exposed *A. torulosa* cells. (F) Transmission electron micrographs of thin sections of *A. torulosa* cells before and after 120 h U exposure. The uranyl phosphate precipitates (indicated with arrows) were found to be scattered around the degraded cell aggregates. Uranyl composition of the precipitates was previously confirmed by energy dispersive X-ray fluorescence (EDXRF) spectroscopy, which revealed all components of uranium L (UL) X rays, i.e., UL_l, ULα, $UL_{\beta 1}$, and $UL_{\beta 2}$.

exposure yielded a spectrum clearly identifiable as hydrated uranyl phosphate species, $H_2(UO_2)_2(PO_4)_2{\cdot}8H_2O$ or chernikovite, a U(VI) autunite-type mineral (International Centre for Diffraction Data [ICDD] file 08-0296) (47, 48) (Fig. 4A). The fluorescence spectrum of bioprecipitated U associated with 120-h U-exposed *A. torulosa* cells recorded with an excitation wavelength of 400 nm revealed fluorescence peaks at 505, 526, 550, and 575 nm, characteristic of chernikovite/meta-autunite (47) in contrast to that from 0- or 24-h U-exposed cells, which did not reveal any such peaks (Fig. 4B). The absence of characteristic fluorescence peaks in 24-h U-exposed culture indicated that uranium colocalization with polyP in 24 h probably did not result in uranyl phosphate precipitates, and that a longer U exposure (120 h) was required for the mineral formation by *A. torulosa* cells via polyP degradation. This is in contrast to the earlier studies where uranium accumulated intracellularly as precipitates closely associated with polyphosphate granules in *Arthrobacter ilicis* when exposed to 336 μM U for 1 h (18).

The X-ray absorption near edge structure (XANES) spectra of the bioprecipitated uranium was observed to be identical to the reference sample of U(VI) carbonate. The absorption edge position in the bioprecipitated or reference sample was consistent

TABLE 1 Structural parameters of the uranium complexes formed by *A. torulosa* cells following 120 h of uranyl exposure[a]

Complex	*R*	N	σ^2
U-O_{ax}	1.73 ± 0.02	2	0.001 ± 0.001
U-O_{eq}	2.26 ± 0.01	3.7 ± 0.3	0.006 ± 0.002
U-P	3.56 ± 0.04	3.7 ± 0.4	0.015 ± 0.005

[a]*R* factor of 0.008.

with uranium in a +6 oxidation state, i.e., U(VI) (49) (Fig. 4C). The k^2-weighted $X(r)$ spectrum obtained from extended X-ray absorption fine structure (EXAFS) analysis and the corresponding Fourier transform (FT) of the uranium complexes formed by *A. torulosa* cells following 120 h of U exposure are presented in Fig. 4D and E, respectively, along with the best theoretical fit obtained from the structure of meta-autunite (50). The parameter results of the quantitative fit along with the errors are provided in Table 1, and the fittings in *k* space and *r* space are included in Fig. 4D and E, respectively. The maximum number of independent points (N_{idp}) (obtained from Nyquist criteria, $N_{idp} = 2\Delta k\Delta r/\pi$, where Δk is the range over which the Fourier transform window is nonzero and Δr is the range over which the fit is evaluated) (51) in the case of EXAFS analysis was found to be 11.15, where $\Delta k = 9 - 2 = 7$ and $\Delta r = 3.5 - 1 = 2.5$. As the same ΔE_0 (correction in edge energy) was used for all the paths, the number of parameters varied in this fit was 9, which was less than the number of independent variables. The best fit consisted of 2.0 axial oxygen atoms, O_{ax}, at a distance of 1.73 Å and 4 equatorial oxygen atoms, O_{eq}, at 2.26 Å (Table 1 and Fig. 4E). The observed U-O_{eq} bond distance of 2.26 Å is well within the range of earlier reported values for the oxygen atoms of phosphate bound to uranyl (52). The best fit for phosphate associated with uranium demonstrated 4 atoms at 3.56 Å (Table 1). This U-P distance is in agreement with monodentate coordination of phosphate to the uranyl equatorial plane similar to meta-autunite (50). Overall, the EXAFS analysis of the bioprecipitated U sample (Table 1 and Fig. 4D and E) showed features and distances for U-O_{ax}, U-O_{eq}, and U-P consistent with that of a meta-autunite-like uranyl phosphate mineral (50, 53).

Transmission electron microscopic (TEM) analysis revealed the extracellular localization of uranyl phosphate precipitates in 120-h U-treated cells (Fig. 4F). These uranyl precipitates appeared as electron-dense needle-like fibrils disseminated in the vicinity of the lysed and decomposed cells of 120-h U-exposed culture in contrast to control, U-unchallenged intact cells (Fig. 4F). TEM observations of extracellular uranyl precipitates around the degraded cells (Fig. 4F) correlate well with that of flask observations (Fig. 3F), where the yellowish, fine, powdery, crystalline uranyl precipitates were found to be scattered at the bottom of the flask beneath the decomposed *A. torulosa* cell aggregates.

Inducible alkaline phosphatase activity, akinete germination, and regeneration of U-exposed *A. torulosa* cells. The expression of alkaline phosphatase (APase) in response to U exposure under phosphate-limited conditions was investigated in *A. torulosa*. Control and U-challenged *A. torulosa* cells revealed minimal basal levels of cell-associated alkaline phosphatase (APase) activity at 24 h, which increased significantly in uranium-exposed cells by 384 h (~84×) compared with that of control U-unchallenged cells which demonstrated an ~27× increase in the activity over the same duration (Fig. 5A). Negligible APase activity was detected in the culture supernatants of control and U-exposed cells, establishing the cell-bound location of APase in *A. torulosa*. A zymogram analysis of U-treated cells showed substantial induction of alkaline phosphatase activity within 192 h of U exposure (the active APase was visualized as multimeric protein), which was found to be stable during 384 h of uranyl exposure (Fig. 5B). On the other hand, APase activity bands were observed only by 288 to 384 h of incubation in control U-unchallenged cells under phosphate-limited conditions (Fig. 5B). Increased alkaline phosphatase (APase) activity and its induction during sporulation under P^- stress was reported in *Anabaena doliolum* (54). We had

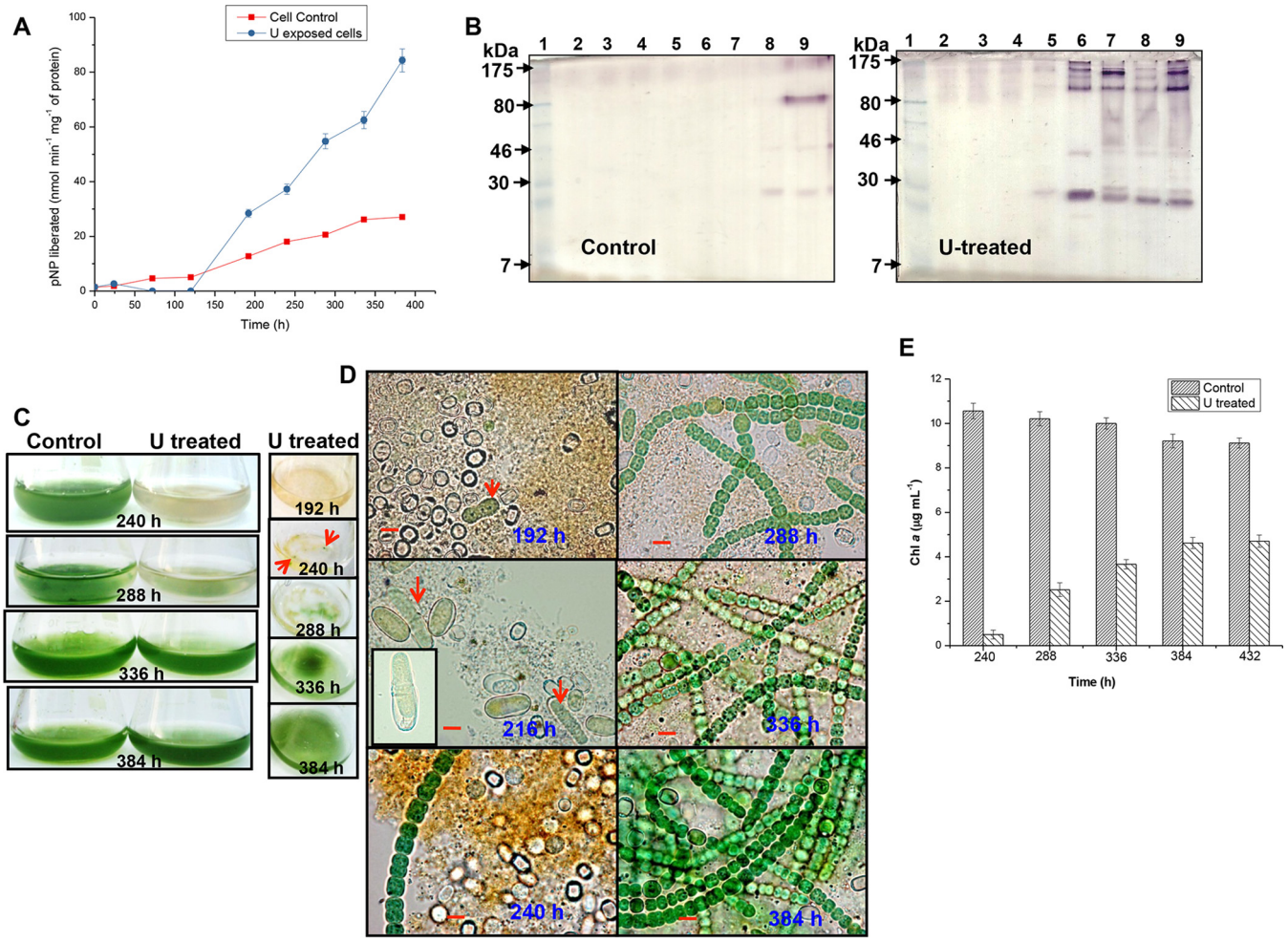

FIG 5 Regeneration of *A. torulosa* following prolonged uranyl exposure. (A) Alkaline phosphatase (APase) activity and the corresponding zymogram (B) of control U-untreated cells or cells treated with 100 μM U at various time points during incubation for up to 384 h. The lanes in the zymogram (B) contained cell extracts from control U-untreated cells and U-treated cells at 0 h (lane 2), 24 h (lane 3), 72 h (lane 4), 120 h (lane 5), 192 h (lane 6), 240 h (lane 7), 288 h (lane 8), and 384 h (lane 9). Protein extracts (corresponding to 50 μg and 28 μg for control and U-treated cells, respectively, except for 19 μg in 288-h U-treated cells) were electrophoretically resolved by nonreducing SDS-PAGE along with prestained molecular mass standards (lane 1) and stained for in-gel phosphatase activity. (C) The flasks containing control U-unchallenged or U-challenged cultures demonstrating the regeneration following 384 h of uranium exposure. Also seen here is a top view of the flasks containing U-exposed cultures at definite intervals. Tiny green patches (marked by red arrows) heralding the regeneration were seen on the top of the experimental solution by 240 h of U exposure. (D) Bright-field microscopy (magnification, ×1,500; bars indicate 5 μm) of regenerating cultures corresponding to those shown in panel C. The germination of the akinetes is visualized by the elongation and division of the spore-like cells (192 h, indicated by red arrow) followed by the emergence of the germling (216 h, indicated by red arrows) comprising 2 to 3 vegetative cells (the inset in the image presents a closer view of the emerging germling). Images corresponding to 240 to 384 h of U exposure represent the progression of the regeneration of the cells. (E) Growth of control and regenerated *A. torulosa* cultures following uranium exposure is represented by chlorophyll *a* contents.

observed akinetes in 96- to 120-h U-exposed *A. torulosa* culture (Fig. 1A), whereas the control U-unexposed culture showed akinete formation only by 384 h of incubation (Fig. 1B) under P-limited conditions. The induction of APase activity has been shown as a biochemical event preceding sporulation under P^- stress in several cyanobacteria (55).

Tiny green patches resembling small flakes typical of actively growing filaments appeared to be floating on the top of the experimental solution in the flask within 240 h of U exposure (Fig. 5C, indicated by arrows). These green patches surrounded by yellowish (bleached) cell aggregates (240 h), when subjected to microscopy, revealed populations of decomposed cells, heterocysts, germinating akinetes, and few intact green filaments, consistent with the characteristic features of a growing culture (Fig. 5D). The soluble inorganic phosphate (Pi) was found to be negligible (0.02 μM) by 192 h in uranium exposed culture compared with ~8.02 μM in the control U-unexposed culture (Table 2). Low soluble concentrations of phosphate (0.9 μM) were shown to

TABLE 2 Stability of uranyl phosphate mineral following regeneration of *A. torulosa* cells

	Control		U treated		
Time (h)	pH	PO_4^{2-} (μM)	pH	PO_4^{2-} (μM)	U (μM)
0	7.2	7.12 ± 0.23	7.8	5.16 ± 0.19	100 ± 5
120	7.2	7.36 ± 0.26	8.2	1.12 ± 0.06	10.2 ± 0.51
192	7.5	8.02 ± 0.39	8.5	0.02 ± 0.001	8.01 ± 0.40
288	7.8	8.14 ± 0.35	8.9	0.02 ± 0.001	7.89 ± 0.39
384	8.2	9.06 ± 0.42	9.2	—[a]	5.0 ± 0.25

[a]—, not available.

induce the germination of akinetes in *Nodularia spumigena* of *Nostocales* (56). The germination of the akinetes in *A. torulosa* observed within 192 to 216 h of U exposure was characterized by elongation and division of the spore-like cell followed by the emergence of the germling, comprising 2 to 3 vegetative cells (Fig. 5D, indicated by arrows) and was similar to that observed in *Aphanizomenon ovalisporum* (a *Nostocales* species like *Anabaena torulosa*) (57, 58). Significant regeneration of *A. torulosa* was observed following 384 h of continuous uranium exposure (Fig. 5C and D). Chlorophyll *a* concentrations increased incrementally from 0.5 μg ml^{-1} at 240 h to 4.62 to 4.7 μg ml^{-1} by 384 to 432 h in U-exposed cells, whereas a marginal decrease in chlorophyll *a* was observed for control cells during the same period (Fig. 5E).

No polyphosphates were visualized in the regenerated or revived filaments of *A. torulosa* subjected to toluidine blue staining, indicative of a polyphosphate-deficient status of the revived cells (Fig. 6A). These cells were found to be extremely sensitive to uranium toxicity and lysed immediately on exposure to 100 μM uranyl carbonate (Fig. 6B). This is in agreement with the observations of polyphosphate-deficient cells of

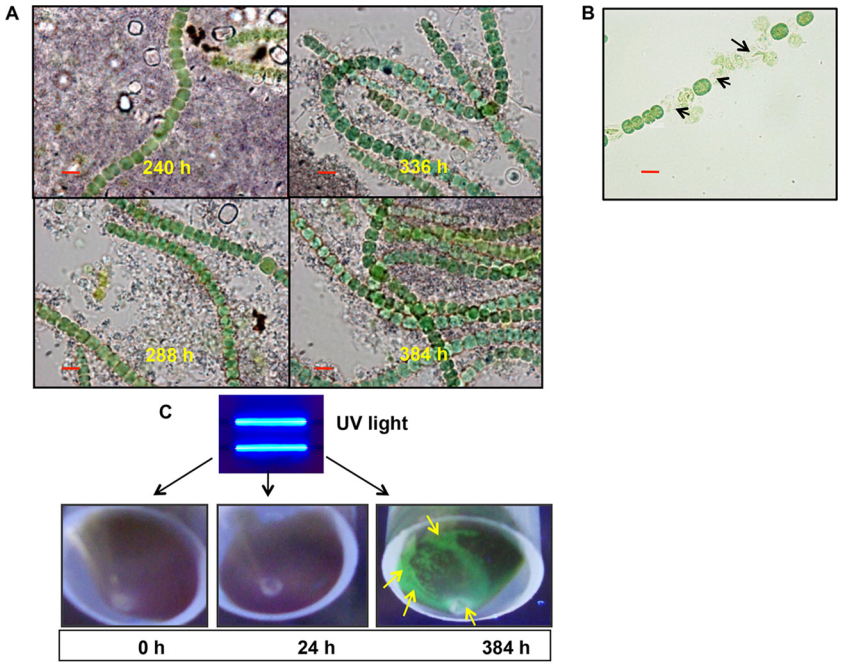

FIG 6 Features of regenerated *A. torulosa* cells and stability of the biomineralized uranyl following cell regeneration. (A) Regenerated cells stained with toluidine blue were observed using bright-field microscopy in a Carl Zeiss Axioskop 40 microscope (Carl Zeiss, Germany) (magnification, ×1,500; bars indicate 5 μm) following 240 to 384 h of uranium exposure. No polyphosphates were visualized in these regenerating cells. (B) Regenerated cells exposed to 100 μM U for 5 min under shaking conditions were observed using bright-field microscopy (bar indicates 5 μm). The regenerated cells showed lysis (marked by black arrows) suggestive of their sensitivity to U toxicity. (C) Cells of *A. torulosa* were incubated with 100 μM U for 0 h, 24 h, or 384 h and the respective cell pellets were exposed to UV light and photographed. The uranyl precipitates at the bottom of the regenerated biomass at 384 h displayed a distinct green fluorescence (marked by yellow arrows) consistent with autunite mineral.

Klebsiella aerogenes, which were found to be very sensitive to cadmium (44). The soluble uranium and phosphate concentrations following uranium precipitation (≥120 h) and cell regeneration (≥192 h) were found to be negligible and remained largely unaltered over the 384 h of uranyl exposure (Table 2), suggesting the stability of uranyl phosphate (autunite) mineral during this period. Uranium release from autunite mineral is known to be stimulated by a decrease in pH (ranging between 2 to 5) due to microbial activities (59). The pH of the lysed/regenerated cultures appended with uranyl precipitates was recorded in the range of 8.2 to 9.2, which is significantly higher than the pH values known for promoting autunite dissolution (Table 2). However, the exact reason for the observed increase in the pH of the regenerated cultures is currently unknown. Cells unexposed to U or exposed to U for 0 h, 24 h, or 384 h were subjected to centrifugation and the resulting cell pellets were exposed to UV light (excitation wavelength [λ_{ex}], 380 nm) (Fig. 6C). The uranyl precipitates settled beneath the regenerated *A. torulosa* cells displayed green-colored fluorescence consistent with autunite mineral (47), thereby establishing the stability of biomineralized U following the regeneration of *A. torulosa* (Fig. 6C). Cells unexposed to U or exposed to U for 24 h did not show any green fluorescence, excluding the possibility of uranium biomineralization in such cells (Fig. 6C).

DISCUSSION

Cyanobacteria are known to be among the first organisms to appear on earth. Having evolved 3.5 billion years ago, cyanobacteria have acquired extremely adaptable ecophysiological traits to compete and survive in harsh environmental conditions (60). The long evolutionary history is a testimony to their remarkable adaptability, thereby presenting them as model organisms to study environmental stress responses. Our findings revealed an interesting cascade of metabolic responses employed by the cells of a naturally occurring, marine, filamentous diazotrophic cyanobacterium, *Anabaena torulosa*, to mitigate sustained U toxicity, concurrently safeguarding its survival over an extended period of U exposure, the results of which have been summarized in Fig. 7.

A. torulosa cells bound 65% of U (15.47 μg ml^{-1}) when challenged with 100 μM (23.8 μg ml^{-1}) uranyl carbonate for 24 h at pH 7.8 (Fig. 3C) and showed the U was concentrated in dense dark granules corresponding to polyphosphate bodies (Fig. 1A). These results are in agreement with our previous observations on uranyl interactions with this cyanobacterium (42, 61). The compartmentalization of uranium in polyphosphates in *A. torulosa* within 24 h of U exposure (Fig. 1A and 3C) made U less available to the cells, thus minimizing U toxicity (42). The incorporation of heavy metals into polyphosphates as a mechanism of metal detoxification has been reported in *Anabaena* cells (41). The diminishing polyP levels under U exposure beyond 24 h suggested that the cells metabolized polyP to maintain their growth under P-limited conditions by degrading their polyphosphates (Fig. 3A and B). It is likely that ~50% degradation in polyphosphate levels by 36 h (Fig. 3A) resulted in the release of uranium complexed to polyphosphates, which, on attaining the cellular toxic threshold levels, caused cell lysis (Fig. 1A and 3B). Growth in the microalga *Selenastrum capricornutum* was shown to be terminated when zinc stored in polyphosphate bodies was released and reached an intracellular toxic threshold as the cells metabolized P for growth under phosphate-limited conditions (62).

The formation of akinetes and their germination through APase activity leading to cell regeneration following uranium biomineralization represent well-orchestrated cellular adaptation of *A. torulosa* cells to overcome sustained uranium toxicity under phosphate limitation. No such phenomenon of cell lysis and its subsequent regeneration in 384 h was observed for control U-unchallenged cells, discounting any possibility of "artifactual" behavior arising as a result of a general stress response under phosphate limitation. The role of cyanobacterial akinetes as resting cells that are able to withstand unfavorable conditions for extended periods of time is well documented (55, 63, 64). The features exhibited by akinetes in U-exposed cultures of *A. torulosa* (Fig. 2) conform to the previously reported observations on akinetes formed by different species of the

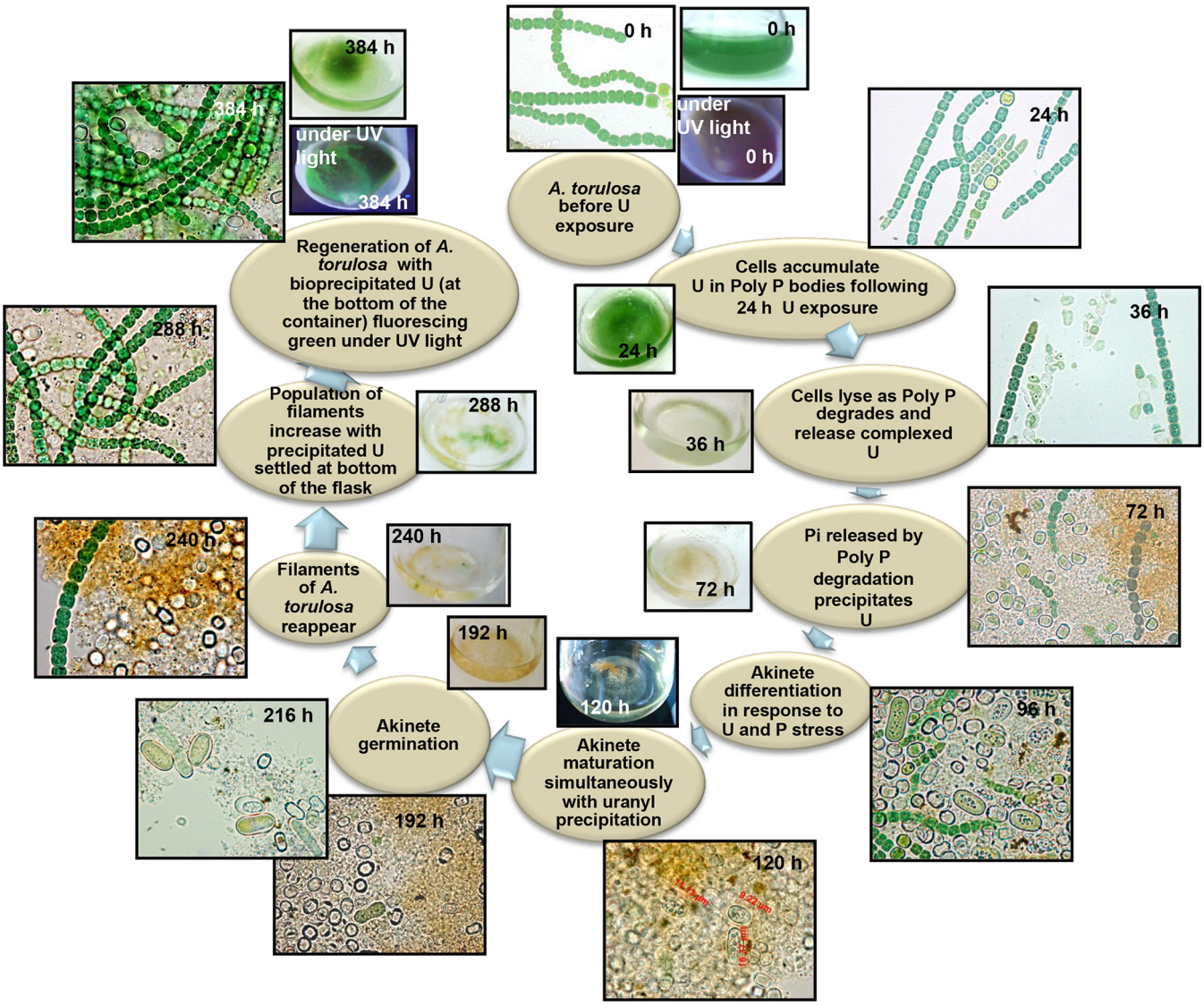

FIG 7 Summary of the events exhibited by *A. torulosa* following exposure to 100 μM uranyl carbonate at pH 7.8 for 384 h, extending from cell lysis to regeneration.

filamentous heterocystous cyanobacteria belonging to *Nostocales* in response to stress, showing (i) viability up to several years, (ii) more tolerance to physical extremes than vegetative cells, and (iii) ready germination when placed under favorable conditions (43, 65–67).

The cyanobacterial adaptations to cope with the phosphate-limited conditions consistent with freshwater bodies or marine waters include akinete differentiation and inducible enzyme (alkaline phosphatase) synthesis to transform organically bound phosphate to a utilizable form (37, 46, 54, 56, 68). For example, the ecophysiological aspects of the *Aphanizomenon ovalisporum* (belonging to *Nostocales*) bloom revealed that the akinetes of the organism distributed in the water column and bottom sediments of Lake Kinneret, Israel, and were formed under unfavorable conditions prevailing in the months of winter and spring, which served as an inoculum for their regeneration/reappearance as a bloom in summer and autumn of the following year (57). While the nitrogen requirement of the developing *Aphanizomenon* population was provided by nitrogen fixation by heterocysts, phosphorus was facilitated by its APase activity under phosphate-limited conditions, which utilized the degradation products of the decomposing cells of a dinoflagellate, *Peridinium gatunense*, as an organic P

substrate (57). In our study, the decomposed or degraded cells (or nucleic acids therein) of *A. torulosa* appeared to serve as the organophosphate substrates for the APases during regeneration. The higher number of heterocysts observed at the earlier stages of *A. torulosa* regeneration (Fig. 5D) suggested nitrogen fixation, which might have been beneficial for the developing culture. No detectable amounts of free or soluble inorganic phosphate were found in regenerating culture solutions, indicating that the phosphate released owing to alkaline phosphatase activity was assimilated by the growing *Anabaena* cells to meet their extreme phosphate requirement under P-limited conditions, and it barely contributed to any further precipitation of uranyl beyond 120 to 192 h of U exposure (Table 2). The regenerated cells did not show the presence of polyphosphate bodies endorsing the great demand of phosphate by the cells for their growth and metabolism during regeneration (Fig. 6A).

In conclusion, our results are the first to show the revival or regeneration of any cyanobacterial strain in the presence of prolonged uranium exposure. It is very important to mention here that the lysed (bleached) and decomposed cells of *A. torulosa* (beyond 36 h of U challenge), if not incubated under stationary conditions, do not revive or regenerate. This observation emphasizes the necessity of the precipitated uranyl to settle in the container, generating a U-"free" environment, which facilitated the akinete germination and subsequent cellular regeneration. The regenerated filaments appeared on the upper region of the experimental medium where no measurable uranium concentrations were recorded. Following its transfer and growth in phosphate-supplemented BG-11 medium for 72 to 96 h, the regenerated culture of *A. torulosa* demonstrated a uranium binding efficiency comparable to that of the normal fresh culture under similar experimental conditions. The regenerated cells removed 63.8% of the uranium from test solutions containing 100 μM uranyl carbonate within 24 h at pH 7.8. The present study is limited to uranium-specific responses in this cyanobacterium. Further studies are required to validate these responses with respect to other toxic contaminants/metals under similar phosphate-limited conditions.

MATERIALS AND METHODS

Culture and growth measurements. The filamentous, heterocystous, nitrogen-fixing, photoautotrophic, marine brackish water cyanobacterium, *Anabaena torulosa* was grown in combined nitrogen-free BG-11 media (69) comprising 0.268 μM EDTA·Na_2, 5.46 μM citric acid, 17.4 μM K_2HPO_4, 30.4 μM $MgSO_4{\cdot}7H_2O$, 24.4 μM $CaCl_2{\cdot}2H_2O$, 16.1 μM $Na_2CO_3{\cdot}H_2O$, 2.73 μM $FeSO_4{\cdot}7H_2O$, and Hoogland's reagent [46.4 μM H_3BO_3, 0.765 μM $ZnSO_4{\cdot}7H_2O$, 1.61 μM $NaMoO_4{\cdot}2H_2O$, 0.316 μM $CuSO_4{\cdot}5H_2O$, 0.168 μM $CO(NO_3)_2{\cdot}6H_2O$] at pH 7.2 under continuous shaking (120 rpm) and illumination (30 μE m^{-2} s^{-1}) at 30°C. *A. torulosa* was isolated earlier in our laboratory from the saline paddy fields of Trombay, Mumbai (38). Growth was measured in terms of chlorophyll *a* content (70) or as absorbance (turbidity) of the cells at 750 nm.

Uranium exposure. Uranium exposure experiments were conducted in nitrogen-supplemented (17.6 mM $NaNO_3$) BG-11 medium lacking phosphate (P^-). Nitrogen-supplemented conditions were found to support better growth of *Anabaena* cells compared with that of nitrogen-deficient conditions in the presence of uranium. Phosphate was omitted to avoid spontaneous precipitation and formation of stable complexes with dihydrogen phosphate and hydrogen phosphate ions $[UO_2(H_2PO_4)_3]^-$ or $[UO_2(HPO_4)_2]^{2-}$ (71, 72). Each assay comprised 10 ml of nitrogen-supplemented BG-11 (P^-) medium with or without 100 μM uranyl carbonate $[UO_2(CO_3)_2]^{2-}$ at pH 7.8. The test solutions were allowed to equilibrate for 30 min after uranyl additions. Cells were harvested in the mid-exponential phase of growth by centrifugation (3,000 $\times$ *g* for 3 min), were washed twice with distilled water, and were used for uranyl exposure studies. Experiments were initiated by inoculating a 5 μg chlorophyll *a* ml^{-1} equivalent of cells into the media in the absence of U (controls) or presence of U (U treated), followed by an incubation up to 36 h under continuous shaking and illumination. Beyond 36 h, the flasks containing control U-unchallenged or U-challenged cultures were incubated under stationary conditions with continuous illumination.

Bright field and fluorescence microscopy. Bright-light and fluorescence microscopy of *A. torulosa* cultures were carried out on a Carl Zeiss Axioskop 40 microscope (Carl Zeiss, Germany), and the images were captured with a charge-coupled device (CCD) Axiocam MRc (Zeiss) camera at $\times$1,500 (oil immersion) magnification. Cells were assessed with fluorescence microscopy by exciting them with green light (λ, 520 nm), which is absorbed by phycocyanin, and visualizing the red chlorophyll *a* fluorescence (λ, 680 nm) arising as a consequence of the resonant energy transfer from phycocyanin to chlorophyll *a*.

Staining and visualization of polyphosphate bodies. The polyphosphate bodies in the vegetative cells were visualized using standard staining procedures. The cells were washed with distilled water, fixed with 3% glutaraldehyde at 4°C for 30 min, and stained for 5 min with 0.05% toluidine blue (adjusted to pH 1.0) (73). Cells stained for polyphosphates were rinsed briefly with 0.1 N HCl and were observed using bright field microscopy using a Carl Zeiss Axioskop 40 microscope (Carl Zeiss, Germany) with oil-

immersion objectives (100×). Polyphosphate bodies or granules stained with toluidine blue show a characteristic red color (due to γ-metachromasia) (73).

Akinete staining and laser scanning confocal microscopy. DAPI is known to form fluorescent complexes with double-stranded DNA. The presence of nucleic acids in akinetes was visualized by DAPI staining (74). *A. torulosa* cells/akinetes exposed to U for 96 h were immersed in DAPI solution (0.6% in water) for 5 min and gently washed with sterile water. The resulting samples were observed under an upright laser scanning confocal microscope (LSM 510 Meta; Carl Zeiss, Germany) using a UV laser source. LSM software supplied with the microscope was used to display a wavelength color-coded view of the nucleic acids in the akinetes.

Assays of uranium, polyphosphate, and inorganic phosphate. Aliquots (100 μl) were withdrawn at timed intervals and centrifuged at 12,000 × *g* for 3 min for the estimation of cell-bound and residual uranium. The uranium-loaded cell pellets (washed with distilled water to remove loosely bound uranium) were digested with 0.2% HCl at room temperature. The supernatants (containing residual uranium) were acidified with 0.01 N HCl to prevent precipitation. Uranyl concentrations in pellets and supernatants were assayed spectrophotometrically using the Arsenazo III method (75).

For the total cellular polyphosphates, control and U-challenged cells (equivalent to 0.2 mg [dry weight] ml^{-1}) were harvested by centrifugation (10,000 × *g* for 10 min) and washed with isotonic saline. Polyphosphates were precipitated and purified from the cells by the ice-cold trichloroacetic acid (TCA) method (76). The purified polyphosphates were hydrolyzed with 1 N HCl at 100°C for 15 min and analyzed for their inorganic phosphate (Pi) contents using a colorimetric (molybdenum blue) method (76). For Pi measurements, test and standard solutions diluted appropriately with distilled water were added to a mixture of 10% ascorbic acid and 0.42% ammonium molybdate (freshly prepared). The resulting reaction mixtures were incubated at 45°C for 20 min, and the absorbances were recorded at 820 nm.

X-ray diffraction analysis. The identity of uranium deposits associated with the cyanobacterial biomass following 120 h of U exposure was confirmed with X-ray powder diffraction (XRD) analysis. U-loaded biomass samples were examined using a high precision Philips powder X-ray diffractometer (model PW 1071) with Ni-filtered Cu-Kα radiation with an exposure time of 2 h. The diffraction pattern was recorded for 2 h from 10 to 70° (2θ) with step length of 0.02° (2θ).

Fluorescence spectroscopy. The fluorescence spectra for cells exposed to uranium for 0 h, 24 h, and 120 h were recorded by means of a Jasco FP-6500 spectrofluorometer (Jasco, Japan) with an excitation wavelength of 400 nm.

X-ray absorption spectroscopy. *A. torulosa* cells exposed to uranium for 120 h were harvested by centrifugation (10,000 × *g* for 10 min) and washed with sterile distilled water to remove interfering ingredients from the growth medium. The cell pellets were dried at 60°C, ground to homogeneity, and analyzed by X-ray absorption near edge structure (XANES) and extended X-ray absorption fine structure (EXAFS) spectroscopy to determine the oxidation state and the neighboring atoms of the complexed uranium, respectively. A solution of 10^{-3} M $[UO_2(CO_3)_2]^{2-}$ served as the reference sample for the oxidation state of uranium, i.e., U(VI) confirmed previously with UV-Vis spectroscopy (72).

Uranium L_{III} edge XAS measurements were carried out in fluorescence mode at the Scanning EXAFS beamline (BL-9) of INDUS-2 synchrotron source (2.5 GeV, 100 mA) at the Raja Ramanna Centre for Advanced Technology (RRCAT), Indore, India (77). The beamline uses a double crystal monochromator (DCM) which works in the photon energy range of 4 to 25 keV with a resolution of 10^4 at 10 keV. The EXAFS spectra of the samples at U L_{III} edge were recorded in the energy range of 17,050 to 17,600 eV and were analyzed according to the standard procedures using the program available within the IFEFFIT software package (78). This included background subtraction, data reduction, and Fourier transform (FT) to derive the FT-EXAFS, $X(r)$ versus radial distance, r spectra from the absorption spectra, generating the theoretical EXAFS spectra starting from an assumed crystallographic structure, and finally fitting of the experimental data with the theoretical spectra using the FEFF 6.0 code. The bond distances, coordination numbers, and disorder (Debye-Waller) factors (σ^2) were used as fitting parameters. The fits were performed in r space with an r range of 1 to 3.5 Å, while a k range of 2 to 9 Å was used for the Fourier transform. The experimental $X(r)$ versus r spectra of the uranium-treated samples at U L_{III} edge were fitted from 1 to 3.5 Å with the theoretical model comprising axial oxygen, U-O_{ax}, and equatorial oxygen, U-O_{eq}, shells and one shell of phosphate, i.e., U-P. During the fitting, the coordination number (N) of the U-O_{ax} bond was held constant at 2. The R (goodness of fit) factor for this fit was found to be 0.008, suggesting a good fit of the data.

Transmission electron microscopy. Control U-unchallenged cells or cells challenged with 100 μM uranyl carbonate for 120 h were washed twice with 50 mM cacodylate buffer (pH 7.4) and fixed in a solution (2.5% glutaraldehyde plus 0.5% formaldehyde) overnight at 4°C (17). Following three washes with cacodylate buffer, cells were embedded in 2% noble agar and dehydrated in a graded series of ethanol (30, 60, 75, 90, and 100%). After removal of the ethanol by treatment with propylene oxide, blocks were subsequently infiltrated with Spurr's reagent on incubation with 1:3, 3:1, and 1:1 (vol/vol propylene oxide/Spurr's reagent) for 2 h each. The samples were finally infiltrated with Spurr's resin for 16 h and embedded in it by incubation at 60°C for 72 h. Thin sections of samples were prepared with a microtome (Leica, Germany) and placed on 200-mesh Formvar-coated copper grids and viewed with a Libra 120 plus transmission electron microscope (Carl Zeiss, Germany) (17).

Alkaline phosphatase expression via activity assays and zymogram. Cell-based alkaline phosphatase activities in untreated and U-treated *A. torulosa* cells were determined with the substrate *para*-nitrophenyl phosphate (*p*-NPP) as described earlier (17). Assays were carried out in 50 mM Tris-Cl buffer (pH 9), and the enzyme activity was expressed as nmol of *para*-nitrophenol (*p*-NP) liberated per

min per mg of total protein. For the zymogram, *A. torulosa* cells/aggregates were washed with distilled water and resuspended in 50 mM Tris-Cl buffer (pH 8.0) and were subjected to repeated freeze-thaw cycles (4 cycles alternating between liquid nitrogen and 37°C). The cell extracts were obtained by centrifugation at 6,000 × *g* for 10 min. Protein concentrations in the cell lysates were determined by a modified Lowry's method (79). An in-gel zymogram assay was carried out by resolving the cell extracts electrophoretically on 12% SDS-PAGE followed by staining with nitro-blue-tetrazolium chloride/5-bromo-4-chloro-3-indolyl phosphate (NBT/BCIP; Roche Chemicals, Germany) in 50 mM Tris-Cl buffer (pH 9) (17).

Statistical analyses. Each experiment comprising three replicates was repeated at least three times. Average values with standard errors are shown for a representative experiment. The variation among different experiments was less than 10%.

ACKNOWLEDGMENTS

We thank R. Vasumathy, Radiation Biology and Health Sciences Division, BARC, and Rakesh R. Shukla, Chemistry Division, BARC, for technical help with confocal microscopy and X-ray diffraction studies of the cyanobacterial samples, respectively. A. Ballal, Alka Gupta, and Namrata A. Waghamare, Molecular Biology Division, BARC, are duly acknowledged for TEM analysis of the cyanobacterial samples. We acknowledge S. K. Apte, HBNI and BARC, for insightful discussions during the early part of this work and S. Chattopadhyay, Bio-Science Group, BARC, for his constant motivation and encouragement during the course of this study.

REFERENCES

1. Cavalier-Smith T. 2006. Cell evolution and Earth history: stasis and revolution. Philos Trans R Soc Lond B Biol Sci 361:969–1006. https://doi.org/10.1098/rstb.2006.1842.
2. Wackett LP, Dodge AG, Ellis LB. 2004. Microbial genomics and the periodic table. Appl Environ Microbiol 70:647–655. https://doi.org/10.1128/AEM.70.2.647-655.2004.
3. Denef VJ, Mueller RS, Banfield JF. 2010. AMD biofilms: using model communities to study microbial evolution and ecological complexity in nature. ISME J 4:599–610. https://doi.org/10.1038/ismej.2009.158.
4. Hemme CL, Deng Y, Gentry TJ, Fields MW, Wu L, Barua S, Barry K, Tringe SG, Watson DB, He Z, Hazen TC. 2010. Metagenomic insights into evolution of a heavy metal-contaminated groundwater microbial community. ISME J 4:660–672. https://doi.org/10.1038/ismej.2009.154.
5. Neu MR, Boukhalfa H, Merroun ML. 2010. Biomineralization and biotransformations of actinide materials. MRS Bull 35:849–857. https://doi.org/10.1557/mrs2010.711.
6. Merroun ML, Selenska-Pobell S. 2008. Bacterial interactions with uranium: an environmental perspective. J Contam Hydrol 102:285–295. https://doi.org/10.1016/j.jconhyd.2008.09.019.
7. Lloyd JR, Gadd GM. 2011. The geomicrobiology of radionuclides. Geomicrobiol J 28:383–386. https://doi.org/10.1080/01490451.2010.547551.
8. Acharya C, Apte SK. 2013. Insights into the interactions of cyanobacteria with uranium. Photosynth Res 118:83–94. https://doi.org/10.1007/s11120-013-9928-9.
9. Newsome L, Morris K, Lloyd JR. 2014. The biogeochemistry and bioremediation of uranium and other priority radionuclides. Chem Geol 363:164–184. https://doi.org/10.1016/j.chemgeo.2013.10.034.
10. Lovley DR, Phillips EJP. 1992. Bioremediation of uranium contamination with enzymatic uranium reduction. Environ Sci Technol 26:2228–2234. https://doi.org/10.1021/es00035a023.
11. Lloyd JR, Chesnes J, Glasauer S, Bunker DJ, Livens FR, Lovley DR. 2002. Reduction of actinides and fission products by Fe(III)-reducing bacteria. Geomicrobiol J 19:103–120. https://doi.org/10.1080/014904502317246200.
12. Williamson AJ, Morris K, Law GT, Rizoulis A, Charnock JM, Lloyd JR. 2014. Microbial reduction of U(VI) under alkaline conditions: implications for radioactive waste geodisposal. Environ Sci Technol 48:13549–13556. https://doi.org/10.1021/es5017125.
13. Lovley DR, Roden EE, Phillips EJP, Woodward JC. 1993. Enzymatic iron and uranium reduction by sulphate-reducing bacteria. Mar Geol 113:41–53. https://doi.org/10.1016/0025-3227(93)90148-O.
14. Bernier-Latmani R, Veeramani H, Vecchia ED, Junier P, Lezama-Pacheco JS, Suvorova EJ, Sharp JO, Wigginton NS, Bargar JR. 2010. Non-uraninite products of microbial U(VI) reduction. Environ Sci Technol 44:9456–9462. https://doi.org/10.1021/es101675a.
15. Macaskie LE, Bonthrone KM, Yong P, Goddard DT. 2000. Enzymically mediated bioprecipitation of uranium by a *Citrobacter* sp.: a concerted role for exocellular lipopolysaccharide and associated phosphatase in biomineral formation. Microbiology 146:1855–1867. https://doi.org/10.1099/00221287-146-8-1855.
16. Macaskie LE, Empson RM, Cheetham AK, Grey CP, Skarnulis AJ. 1992. Uranium bioaccumulation by a *Citobacter* sp. as a result of enzymically mediated growth of polycrystalline HUO_2PO_4. Science 257:782–784. https://doi.org/10.1126/science.1496397.
17. Kulkarni S, Ballal A, Apte SK. 2013. Bioprecipitation of uranium from alkaline waste solutions using recombinant *Deinococcus radiodurans*. J Hazard Mater 262:853–861. https://doi.org/10.1016/j.jhazmat.2013.09.057.
18. Suzuki Y, Banfield JF. 2004. Resistance to, and accumulation of, uranium by bacteria from a uranium-contaminated site. Geomicrobiol J 21:113–121. https://doi.org/10.1080/01490450490266361.
19. Kornberg A, Rao NN, Ault-Riche D. 1999. Inorganic polyphosphate: a molecule of many functions. Annu Rev Biochem 68:89–125. https://doi.org/10.1146/annurev.biochem.68.1.89.
20. Merroun M, Hennig C, Rossberg A, Reich T, Selenska-Pobell S. 2003. Characterization of U(VI)-*Acidithiobacillus ferrooxidans* complexes using EXAFS, transmission electron microscopy, and energy-dispersive X-ray analysis. Radiochim Acta 91:583–591. https://doi.org/10.1524/ract.91.10.583.22477.
21. Merroun ML, Nedelkova M, Rossberg A, Hennig C, Selenska-Pobell S. 2006. Interaction mechanisms of bacterial strains isolated from extreme habitats with uranium. Radiochim Acta 94:723–729. https://doi.org/10.1524/ract.2006.94.9-11.723.
22. Suzuki Y, Banfield JF. 1999. Geomicrobiology of uranium. Rev Mineral Geochem 38:393–432.
23. Boswell CD, Dick RE, Macaskie LE. 1999. The effect of heavy metals and other environmental conditions on the anaerobic phosphate metabolism of *Acinetobacter johnsonii*. Microbiology 145:1711–1720. https://doi.org/10.1099/13500872-145-7-1711.
24. Renninger N, Knopp R, Nitsche H, Clark D, Keasling J. 2004. Uranyl precipitation by *Pseudomonas aeruginosa* via controlled polyphosphate metabolism. Appl Environ Microbiol 70:7404–7412. https://doi.org/10.1128/AEM.70.12.7404-7412.2004.
25. Martinez RJ, Beazley MJ, Taillefert M, Arakaki AK, Skolnick J, Sobecky PA. 2007. Aerobic uranium (VI) bioprecipitation by metal-resistant bacteria isolated from radionuclide- and metal-contaminated subsurface soils. Environ Microbiol 9:3122–3133. https://doi.org/10.1111/j.1462-2920.2007.01422.x.
26. Sivaswamy V, Boyanov MI, Peyton BM, Viamajala S, Gerlach R, Apel WA, Sani RK, Dohnalkova A, Kemner KM, Borch T. 2011. Multiple mechanisms of uranium immobilization by *Cellulomonas* sp. strain ES6. Biotechnol Bioeng 108:264–276. https://doi.org/10.1002/bit.22956.
27. Beazley MJ, Martinez RJ, Sobecky PA, Webb SM, Taillefert M. 2007. Uranium biomineralization as a result of bacterial phosphatase activity:

insights from bacterial isolates from a contaminated subsurface. Environ Sci Technol 41:5701–5707. https://doi.org/10.1021/es070567g.
28. Lovley DR, Phillips EJP, Gorby YA, Landa ER. 1991. Microbial reduction of uranium. Nature 350:413–416. https://doi.org/10.1038/350413a0.
29. Wu WM, Carley J, Gentry T, Ginder-Vogel MA, Fienen M, Mehlhorn T, Yan H, Caroll S, Pace MN, Nyman J, Luo J. 2006. Pilot-scale in situ bioremediation of uranium in a highly contaminated aquifer. 2. Reduction of U(VI) and geochemical control of U(VI) bioavailability. Environ Sci Technol 40:3986–3995.
30. Newsome L, Morris K, Lloyd JR. 2015. Uranium biominerals precipitated by an environmental isolate of *Serratia* under anaerobic conditions. PLoS One 10:e0132392. https://doi.org/10.1371/journal.pone.0132392.
31. Langmuir D. 1978. Uranium solution-mineral equilibria at low temperatures with applications to sedimentary ore deposits. Geochim Cosmochim Acta 42:547–569. https://doi.org/10.1016/0016-7037(78)90001-7.
32. Wu J, Sunda W, Boyle EA, Karl DM. 2000. Phosphate depletion in the western North Atlantic Ocean. Science 289:759–762. https://doi.org/10.1126/science.289.5480.759.
33. Zubkov MV, Mary I, Woodward EM, Warwick PE, Fuchs BM, Scanlan DJ, Burkill PH. 2007. Microbial control of phosphate in the nutrient-depleted North Atlantic subtropical gyre. Environ Microbiol 9:2079–2089. https://doi.org/10.1111/j.1462-2920.2007.01324.x.
34. N'Guessan AL, Elifantz H, Nevin KP, Mouser PJ, Methé B, Woodard TL, Manley K, Williams KH, Wilkins MJ, Larsen JT, Long PE. 2010. Molecular analysis of phosphate limitation in Geobacteraceae during the bioremediation of a uranium-contaminated aquifer. ISME J 4:253–266. https://doi.org/10.1038/ismej.2009.115.
35. Nikata T, Sakai Y, Shibata K, Kato J, Kuroda A, Ohtake H. 1996. Molecular analysis of the phosphate specific transport (pst) operon of *Pseudomonas aeruginosa*. Mol Gen Genet 250:692–698. https://doi.org/10.1007/BF02172980.
36. Santos-Beneit F. 2015. The Pho regulon: a huge regulatory network in bacteria. Front Microbiol 6:402. https://doi.org/10.3389/fmicb.2015.00402.
37. Stihl A, Sommer U, Post AF. 2001. Alkaline phosphatase activities among populations of the colony-forming diazotrophic cyanobacterium *Trichodesmium* spp. (Cyanobacteria) in the Red Sea. J Phycol 37:310–317. https://doi.org/10.1046/j.1529-8817.2001.037002310.x.
38. Fernandes TA, Thomas J. 1982. Control of sporulation in the filamentous cyanobacterium *Anabaena torulosa*. J Biosci 4:85–94. https://doi.org/10.1007/BF02702584.
39. Fernandes TA, Iyer V, Apte SK. 1993. Differential responses of nitrogen-fixing cyanobacteria to salinity and osmotic stresses. Appl Environ Microbiol 59:899–904.
40. Singh H, Fernandes T, Apte SK. 2010. Unusual radioresistance of nitrogen-fixing cultures of *Anabaena* strains. J Biosci 35:427–434. https://doi.org/10.1007/s12038-010-0048-9.
41. Rai LC, Jensen TE, Rachlin JW. 1990. A morphometric and X-ray energy dispersive analysis approach to monitoring pH-altered cadmium toxicity in *Anabaena flos-aquae*. Arch Environ Contam Toxicol 19:479–487. https://doi.org/10.1007/BF01059065.
42. Acharya C, Chandwadkar P, Apte SK. 2012. Interaction of uranium with a filamentous, heterocystous, nitrogen-fixing cyanobacterium, *Anabaena torulosa*. Bioresour Technol 116:290–294. https://doi.org/10.1016/j.biortech.2012.03.068.
43. Sukenik A, Kaplan-Levy RN, Welch JM, Post AF. 2012. Massive multiplication of genome and ribosomes in dormant cells (akinetes) of *Aphanizomenon ovalisporum* (Cyanobacteria). ISME J 6:670–679. https://doi.org/10.1038/ismej.2011.128.
44. Aiking H, Stijnman A, van Garderen C, van Heerikhuizen H, van't Riet J. 1984. Inorganic phosphate accumulation and cadmium detoxification in *Klebsiella aerogenes* CTC 418 growing in continuous culture. Appl Environ Microbiol 47:374–377.
45. Boswell CD, Dick RE, Eccles H, Macaskie LE. 2001. Phosphate uptake and release by *Acinetobacter johnsonii* in continuous culture and coupling of phosphate release to heavy metal accumulation. J Ind Microbiol Biotechnol 26:333–340. https://doi.org/10.1038/sj.jim.7000139.
46. Teikari J, Österholm J, Kopf M, Battchikova N, Wahlsten M, Aro E-M, Hess WR, Sivonen K. 2015. Transcriptomic and proteomic profiling of *Anabaena* sp. strain 90 under inorganic phosphorus stress. Appl Environ Microbiol 81:5212–5222. https://doi.org/10.1128/AEM.01062-15.
47. Haverbeke LV, Vochten R, Springel KV. 1996. Solubility and spectrochemical characteristics of synthetic chernikovite and meta-ankoleite. Mineral Mag 60:759–766. https://doi.org/10.1180/minmag.1996.060.402.05.
48. Nilgiriwala KS, Alahari A, Rao AS, Apte SK. 2008. Cloning and overexpression of an alkaline phosphatase PhoK from *Sphingomonas* sp. BSAR-1 for uranium bioprecipitation from alkaline solutions. Appl Environ Microbiol 74:5516–5523. https://doi.org/10.1128/AEM.00107-08.
49. Hudson EA, Allen PG, Terminello LJ, Denecke MA, Reich T. 1996. Polarized X-ray absorption spectroscopy of the uranyl ion: comparison of experiment and theory. Phys Rev B Condens Matter 54:156–165. https://doi.org/10.1103/PhysRevB.54.156.
50. Merroun ML, Raff J, Rossberg A, Hennig C, Reich T, Selenska-Pobell S. 2005. Complexation of uranium by cells and S-layer sheets of *Bacillus sphaericus* JG-A12. Appl Environ Microbiol 71:5532–5543. https://doi.org/10.1128/AEM.71.9.5532-5543.2005.
51. Kelly SD, Hesterberg D, Ravel B. 2008. Analysis of soils and minerals using X-ray absorption spectroscopy, p 387–464. *In* Ulery AL, Drees R (ed), Methods of soil analysis. Part 5—mineralogical methods. American Society of Agronomy, Madison, WI.
52. Kelly SD, Kemner KM, Fein JB, Fowle DA, Boyanov MI, Bunker BA. 2002. X-ray absorption fine structure determination of pH-dependent U-bacterial cell wall interactions. Geochim Cosmochim Acta 66:3855–3871. https://doi.org/10.1016/S0016-7037(02)00947-X.
53. Hennig C, Panak PJ, Reich T, Rossberg A, Raff J, Selenska-Pobell S, Matz W, Bucher JJ, Bernhard G, Nitsche H. 2001. EXAFS investigation of uranium(VI) complexes formed at *Bacillus cereus* and *Bacillus sphaericus* surfaces. Radiochim Acta 89:625–631. https://doi.org/10.1524/ract.2001.89.10.625.
54. Pandey KD, Sarkar S, Kashyap AK. 1991. Role of inorganic phosphate and alkaline phosphatase in sporulation of *Anabaena doliolum*. Biochem Physiol Pflanz 187:439–445. https://doi.org/10.1016/S0015-3796(11)80052-1.
55. Adams DG, Carr NG. 1981. The developmental biology of heterocyst and akinete formation in cyanobacteria. Crit Rev Microbiol 9:45–100. https://doi.org/10.3109/10408418109104486.
56. Huber AL. 1985. Factors affecting the germination of akinetes of *Nodularia spumigena* (*Cyanobacteriaceae*). Appl Environ Microbiol 49:73–78.
57. Hadas O, Pinkas R, Delphine E, Vardi A, Kaplan A, Sukenik A. 1999. Limnological and ecophysiological aspects of *Aphanizomenon ovalisporum* bloom in Lake Kinneret, Israel. J Plankton Res 21:1439–1453. https://doi.org/10.1093/plankt/21.8.1439.
58. Kaplan-Levy RN, Hadas O, Summers ML, Rucker J, Sukenik A. 2010. Akinetes: dormant cells of cyanobacteria, p 5–27. *In* Lubzens E, Cerda J, Clark M (ed), Dormancy and resistance in harsh environments. Springer, Berlin, Germany.
59. Wellman DM, Gunderson KM, Icenhower JP, Forrester SW. 2007. Dissolution kinetics of synthetic and natural meta-autunite minerals, $\dot{X}((n)+)3-n[(UO_2)(PO_4)]_2{\cdot}H_2O$, under acidic conditions. Geochem Geophys Geosyst 8:1–16. https://doi.org/10.1029/2007GC001695.
60. Litchman E, de Tezanos Pinto P, Klausmeier CA, Thomas MK, Yoshiyama K. 2010. Linking traits to species diversity and community structure in phytoplankton. Hydrobiologia 653:15–28. https://doi.org/10.1007/s10750-010-0341-5.
61. Acharya C, Apte SK. 2013. Novel surface associated polyphosphate bodies sequester uranium in the filamentous, marine cyanobacterium, *Anabaena torulosa*. Metallomics 5:1595–1598. https://doi.org/10.1039/c3mt00139c.
62. Kuwabara JS. 1985. Phosphorus-zinc interactive effects on growth by *Selenastrum capricornutum* (Chlorophyta). Environ Sci Technol 19:417–421. https://doi.org/10.1021/es00135a005.
63. Roelofs TD, Oglesby RT. 1970. Ecological obersevations on the planktonic cyanophyte *Gleotrichia echinulata*. Limnol Oceanogr 15:224–229. https://doi.org/10.4319/lo.1970.15.2.0224.
64. Reynolds CS. 1975. Interactions of photosynthetic behavior and buoyancy regulation in a natural population of a blue-green alga. Freshw Biol 5:323–338. https://doi.org/10.1111/j.1365-2427.1975.tb01759.x.
65. Yamamoto Y. 1976. Effect of some physical and chemical factors on the germination of akinetes of *Anabaena cylindrica*. J Gen Appl Microbiol 22:311–323. https://doi.org/10.2323/jgam.22.311.
66. Sutherland JM, Herdman M, Stewart WDP. 1979. Akinetes of the cyanobacterium, Nostoc PCC 7524: macromolecular composition, structure and control of differentiation. Microbiology 115:273–287. https://doi.org/10.1099/00221287-115-2-273.
67. Livingstone D, Jaworski GHM. 1980. The viability of akinetes of blue-

green algae recovered from the sediments of Rostherne Mere. Eur J Phycol 15:357–364. https://doi.org/10.1080/00071618000650361.
68. Simon RD. 1977. Sporulation in the filamentous cyanobacterium *Anabaena cylindrica*. The course of spore formation. Arch Microbiol 111:283–288. https://doi.org/10.1007/BF00549367.
69. Allen MM. 1968. Simple conditions for the growth of unicellular blue-green algae on plates. J Phycol 4:1–4. https://doi.org/10.1111/j.1529-8817.1968.tb04667.x.
70. Mackinney G. 1941. Absorption of light by chlorophyll solutions. J Biol Chem 140:315–322.
71. Nakajima A, Horikoshi T, Sakaguchi T. 1982. Studies on the accumulation of heavy metal elements in biological systems. XXI. Recovery of uranium by immobilized microorganisms. Appl Microbiol Biotechnol 16:88–91. https://doi.org/10.1007/BF00500732.
72. Acharya C, Joseph D, Apte SK. 2009. Uranium sequestration by marine cyanobacterium, Synechococcus elongatus strain BDU/75042. Bioresour Technol 100:2176–2181. https://doi.org/10.1016/j.biortech.2008.10.047.
73. Ashford AE, Lee ML, Chilvers GA. 1975. Polyphosphate in eucalypt mycorrhizas: a cytochemical demonstration. New Phytol 74:447–453. https://doi.org/10.1111/j.1469-8137.1975.tb01356.x.
74. Porter KJ, Feig YS. 1980. DAPI for identifying and counting aquatic microflora. Limnol Oceanogr 25:943–948. https://doi.org/10.4319/lo.1980.25.5.0943.
75. Savvin SB. 1961. Analytical use of arsenazo III: determination of thorium, zirconium, uranium and rare earth elements. Talanta 8:673–685. https://doi.org/10.1016/0039-9140(61)80164-1.
76. Rao N, Roberts M, Torriani A. 1985. Amount and chain length of polyphosphates in *Escherichia coli* depend on growth conditions. J Bacteriol 162:242–247.
77. Gaur A, Dar DA, Shrivastava BD, Jha SN, Bhattacharyya D. 2015. Performance of BL-8 dispersive and BL-9 scanning EXAFS beamlines at Indus-2 synchrotron. Indian J Phys 89:453–462. https://doi.org/10.1007/s12648-014-0610-7.
78. Newville M, Ravel B, Haskel D, Rehr JJ, Stern EA, Yacoby Y. 1995. Analysis of multiple-scattering XAFS data using theoretical standards. Physica B Condens Matter 208–209:154–155. https://doi.org/10.1016/0921-4526(94)00655-F.
79. Peterson GL. 1977. A simplification of the protein assay method of Lowry et al. which is more generally applicable. Anal Biochem 83:346–356. https://doi.org/10.1016/0003-2697(77)90043-4.